Retrievals of Profiles of Fine and Coarse Aerosols Using Lidar and Radiometric Space Measurements

Yoram J. Kaufman, Didier Tanré, Jean-François Léon, and Jacques Pelon

***Abstract*—The Cloud-Aerosol Lidar and Infrared Pathfinder Satellite Observations (CALIPSO) spaceborne lidar, expected to be launched in 2004, will collect profiles of the lidar attenuated backscattering coefficients of aerosol and clouds at 0.53 and 1.06 μm. The measurements are sensitive to the vertical distribution of aerosols. However, the information is insufficient to be mapped into unique aerosol physical properties and vertical distribution. Spectral radiances measured by the Moderate Resolution Imaging Spectrometer (MODIS) on the Aqua spacecraft, acquired simultaneously with the CALIPSO observations, can constrain the solutions. The combination of the MODIS and CALIPSO data can be used to derive extinction profiles of the fine and coarse modes of the aerosol size distribution for aerosol optical thickness of 0.1 and larger. Here we describe a new inversion method developed to invert simultaneously MODIS and CALIPSO data over glint-free ocean. The method is applied to aircraft lidar and MODIS data collected over a dust storm off the coast of West Africa during the Saharan Dust Experiment (SHADE). The backscattering-to-extinction ratio (BER) (BER $= \omega_o P(180)/4\pi$) can be retrieved from the synergism between measurements avoiding *a priori* hypotheses required for inverting lidar measurements alone. For dust, the resultant value of BER $= 0.016$ sr^{-1} is over 50% smaller than what is expected using Mie theory, but in good agreement with recent results obtained from Raman lidar observations of dust episodes. The inversion is robust in the presence of 10% and 20% noise in the lidar signal at 0.53 and 1.06 μm, respectively. Calibration errors of the lidar of 5% to 10% can cause an error in optical thickness of 20% to 40%, respectively, in the tested cases.**

***Index Terms*—Aerosol, lidar, remote sensing.**

I. Introduction

THE CLOUD-Aerosol Lidar and Infrared Pathfinder Satellite Observations (CALIPSO) spaceborne lidar, expected to be launched in 2004, will collect profiles of the lidar attenuated backscattering coefficients of aerosol and clouds at 0.53 and 1.06 μm. It will fly in formation with the Aqua mission with a Moderate resolution Imaging Spectroradiometer (MODIS) instrument onboard. Analysis of the spaceborne dual wavelength lidar data combined with spectral passive measurements from MODIS will generate a dataset that combines the vertical profile information from CALIPSO with the detailed size information in the MODIS data. Both CALIPSO satellite and MODIS on the Aqua satellite will fly in formation, observing the same spot on the ground within a few minutes. It is expected to resolve to a large extent the ambiguity in deriving the aerosol profile from the lidar measurements.

Detailed profiles of aerosols and clouds, distinguishing fine from coarse aerosol particles, is needed to understand the effect of aerosol on cloud microphysics and precipitation (see review by Kaufman *et al.* [1]). The profile of the aerosol is needed to know if and to what degree the aerosol interacts with the cloud layer. Distinguishing between the fine and coarse aerosol modes in each layer is important in order to understand the effect of the aerosol on cloud properties. For example, high concentrations of fine aerosols can reduce the size of cloud droplets, increase their reflectance [2] and reduce precipitation [3]. However, introduction of large hygroscopic aerosols even in minute numbers can reverse some of these effects [4], allowing precipitation and cleaning of the atmosphere from the fine aerosols [5]. Resolving these effects is needed in order to understand climate change [6] and to predict human effects on precipitation and availability of fresh water [7].

The vertical distribution of the fine aerosols is also important for a different reason. Fine aerosol emitted as smoke from fires or as pollution from populated areas carry with them black carbon particles emitted from fires and "dirty" engines [8]. Black carbon accounts for most of the absorption by fine aerosols, which can be between 3% and 15% of the aerosol extinction optical thickness. High levels of absorption (10% to 15% of the optical thickness) were predicted by climate models to cause increased precipitation and floods in southeast China [9], while causing droughts in the Mediterranean region [10]. The drought in the Mediterranean region was caused by decrease of irradiation of the Mediterranean Sea and reduction of evaporation, without a nearby ocean to supply the missing moisture. The increase in precipitation over southeast China is caused by changes in regional and global circulation, due to the heating of the atmosphere by the black carbon, and influx of moist air from the nearby Pacific ocean. This effect on circulation depends on the height in which the heat is released, and, therefore, on the height of the aerosol layer. Another question related to the injection of aerosol in the upper troposphere is their possible role as ice nuclei. Cirrus clouds have an important greenhouse impact, and their microphysics depends on the conditions under which crystals form. Particles may thus significantly contribute to the modification of cirrus properties via heterogeneous freezing.

There are several complementary differences between the way MODIS and CALIPSO observe aerosol. Over the oceans MODIS measures sunlight backscattered by the atmosphere in eight spectral channels from 0.41–2.1 μm. The MODIS short

Manuscript received June 19, 2002; revised March 27, 2003.

Y. J. Kaufman is with the Climate and Radiation Branch, Goddard Space Flight Center, Greenbelt, MD 20771 USA.

D. Tanré and J.-F. Léon are with the Laboratory d' Optique Atmosphere, CNRS, Universite de Sciences et Techniques de Lille, 59655 Villeneuve d'Ascq, France.

J. Pelon is with the Service d' Aéronomie, Institute Pierre Simon Laplace, Universite Pierre de Marie Curie, 75252 Paris, France.

Digital Object Identifier 10.1109/TGRS.2003.814138

wavelengths are sensitive to scattering by both fine and coarse particles, while the long wavelengths are sensitive mainly to scattering by the coarse particles [11], [12]. This information is used to derive the aerosol optical thickness of the entire atmospheric column separately for the fine and coarse aerosols.

Different physical processes control the formation and removal of the fine and coarse modes, defining a specific range for their size distributions in the atmosphere [13]. The fine mode formed by condensation and oxidation of gases into liquids results in particles with effective radii mainly in the 0.1–0.25-μm range [14], [15]. Coarse particles, formed in physical processes of formation of desert dust and sea spray, have effective radii usually of 1 μm and larger [16]. Therefore, in the inversion of the MODIS data we were able to use a limited set of aerosol sizes [11] by imposing "real-world" restrictions on the solutions, to narrow the range of the mathematical possibilities. We use a database of aerosol size distributions derived from the Aerosol Robotic Network (AERONET) sun and sky measurements [16]–[18] over the last six years from up to 100 stations worldwide, to formulate the restrictions on the size distribution.

MODIS is sensitive to aerosols integrated on the entire atmospheric column and cannot resolve the aerosol profile. The CALIPSO lidar will resolve the vertical distribution of the attenuated aerosol backscattering coefficients using two spectral channels at 0.53 and 1.06 μm, and therefore, can be used to resolve two pieces of information about the aerosol in each layer. MODIS 6 spectral channels used for remote sensing of aerosol over the glint-free ocean can resolve two to three pieces of information about the aerosol size and optical thickness [19]. We chose, therefore, to use MODIS to determine the size of the fine and coarse aerosol modes, and CALIPSO to determine the extinction coefficient of the fine and coarse modes independently in each layer. This does not leave room to resolve variations in the size of the fine or coarse modes with altitude due to effects of humidity or gravitational settling. Such determination would require a third independent wavelength of the lidar (e.g., at 1.6 or 2.1 μm), not planned presently for space missions. By using two rather than three pieces of information from MODIS, we have the additional degree of freedom to check if the system of measurements is consistent. For a well-calibrated lidar with errors smaller than 5%, we can use this information to check if nonsphericity of the particles affects the aerosol properties.

MODIS observations are for variety of scattering angles, while CALIPSO measurements are for a fixed scattering angle of 180°. The differences in the scattering angles and the difference in the sensitivity to aerosol properties (size, refractive index) of the MODIS and CALIPSO measurements makes the integrated dataset of MODIS+CALIPSO lidar a powerful database to resolve aerosol properties.

In this paper, we shall describe and test a new procedure that combines two active wavelength backscattering lidar measurements from aircraft (simulating CALIPSO) with the passive spectral radiometer (MODIS) observations from space. Eventual integration with Polarization and Directionality of Earth Reflectances (POLDER) and lidar depolarization is expected to generate more refined results. This is one of the first attempts to invert simultaneously spaceborne active and passive measurements. Leon *et al.* [20] describe a different technique to invert passive and active measurements from space, by constraining the lidar inversion using MODIS-derived optical thicknesses as well as spectral radiances. The closest publication to our topic is probably the inversion of integrated ground-based measurements of multispectral lidar data and profile spectral extinction coefficient derived from Raman lidar data reported by Müller *et al.*, [21] and Bockmann [22]. Other papers suggested the use of optical thickness derived from satellites [23] or from the ground to constrain the lidar retrievals [24], [25], e.g., from the vast array of ground-based Aerosol Robotic Network (AERONET instruments [26]).

After a brief analysis of information content of MODIS and lidar data, we present the inversion scheme used for combining the two datasets. Data acquired during the SHADE campaign [27] are then used to show the feasibility of the inversion. Sensitivity and errors are discussed in the last section.

TABLE I

EXAMPLE OF FOUR AEROSOL SIZE DISTRIBUTIONS THAT DEMONSTRATES THE IMPORTANCE OF MODIS TO DISENTANGLE THE AEROSOL PROPERTIES. THE AEROSOL SIZE DISTRIBUTION IS COMPOSED OF TWO LOG-NORMAL MODES, FINE AND COARSE, WITH EFFECTIVE RADIUS R_{eff} OF EACH MODE GIVEN IN THE TABLE. THE WIDTH OF THE DISTRIBUTION IS 0.4 FOR THE FINE MODE AND 0.6 FOR THE COARSE MODE. THE CONTRIBUTION OF EACH MODE TO THE OPTICAL THICKNESS AT 0.53 μm IS GIVEN FOR EACH MODE. THE SIZE DISTRIBUTIONS WERE CHOSEN TO GIVE THE SAME RATIO OF THE AEROSOL REFLECTED RADIANCE AT SCATTERING ANGLE OF 180° BETWEEN 1.06 AND 0.53 μm, AND THEREFORE SAME SPECTRAL RATIO OF THE LIDAR BACKSCATTERING COEFFICIENTS. THE RADIANCE AT 2.1 μm RELATIVE TO THAT AT 0.53 μm, MEASURED BY MODIS, DIFFERS FROM ONE DISTRIBUTION TO ANOTHER AND CAN BE USED TO DISTINGUISH AMONG THEM. THE RADIANCES ARE NORMALIZED TO 1ß.0 AT 0.53 μm

	Fine mode		Coarse mode			Normalized aerosol radiance	
	R_{eff} µm	Contribution %	R_{eff}, µm	Contribution %	0.53 µm	1.06 µm	2.13 µm
Case 1	0.15	50	1.0	50	1.00	0.693	0.357
Case 2	0.20	60	1.0	40	1.00	0.690	0.331
Case 3	0.25	69	1.0	31	1.00	0.689	0.309
Case 4	0.20	63	1.5	37	1.00	0.697	0.400

II. INFORMATION CONTENT

A simple demonstration of the information content of the MODIS spectral channels, and their importance to the analysis of CALIPSO data is presented in Table I. The aerosol radiance is the difference between the radiance at the top of the atmosphere with and without aerosol. In this example, a baseline model (case 1) is introduced, with 50% of the optical thickness (at 0.53 μm) due to fine aerosol (effective radius: $R^f_{\text{eff}} = 0.15\,\mu$m) and 50% due to coarse-mode aerosol ($R^c_{\text{eff}} = 1\,\mu$m). For this model, the aerosol radiance at 1.06 μm is 69% of that at 0.53 μm. A change in the size of the fine- or coarse-mode particles from the baseline model can still give the same wavelength dependence between these two wavelengths by adjusting the relative concentration of the two modes. We show (case 2) that the same wavelength dependence between the lidar 0.53- and 1.06-μm channels can be obtained also for a larger fine

mode ($R^f_{\text{eff}} = 0.20\,\mu$m), compensating it with a smaller fraction of the coarse mode (40% instead of 50%). Even larger fine mode (case 3; $R^f_{\text{eff}} = 0.25\,\mu$m) or larger coarse mode (case 4; $R^c_{\text{eff}} = 1.5\,\mu$m) can also generate the same wavelength dependence with, respectively, 31% and 37% coarse mode. Therefore, the lidar backscattering return, proportional to the aerosol radiance for the scattering angle of 180°, cannot distinguish between these four cases. However, the longer MODIS wavelengths (2.13 μm in this case) can distinguish between these cases and resolve the ambiguity about the size and fraction of the modes.

A statistical analysis of the spectral information in the lidar and MODIS data is based on the analysis of Tanré *et al.* [19] for MODIS. It uses single scattering approximation for the aerosol radiance, L, at the top of the atmosphere

$$L(\lambda) = C\tau(\lambda)\omega_o(\lambda)P(\lambda, \Theta) \tag{1}$$

for a range of fine and coarse aerosol modes. Here τ is the optical thickness, ω_o is the single scattering albedo and P the scattering phase function at a scattering angle Θ. C is proportionality constant. The weighting between the two modes is chosen to represent a specific spectral variation of the radiance $L(\lambda)$, expressed by the radiance Ångström exponent function, α_L. For CALIPSO lidar wavelengths of 0.53 and 1.06 μm, we define α_L as the slope of the radiance, with wavelength on a logarithmic scale

$$\alpha_L(0.530/1.06) = -\ln[L(0.53)/L(1.06)]/\ln[0.53/1.06]. \tag{2}$$

From (1) and (2) we get for the single scattering approximation

$$\alpha_L(0.53/1.06) = -\ln\{[\tau(0.53)\omega_o(0.53)P(0.53, \Theta)] /[\tau(1.06)\omega_o(1.06)P(1.06, \Theta)]\}/\ln(0.53/1.06). \tag{3}$$

It is related to the classical Ångström exponent α_τ defined as

$$\alpha_\tau(0.530/1.06) = -\ln[\tau(0.53)/\tau(1.06]/\ln(0.53/1.06) \tag{4}$$

by

$$\alpha_L(0.530/1.06) = \alpha_\tau(0.530/1.06)\ln\{[\omega_o(0.53)/\omega_o(1.06)] \cdot[P(0.53, \Theta)/P(1.06, \Theta)]\}. \tag{5}$$

Fig. 1 shows combinations of the fine and coarse modes that correspond to three fixed values of α_L: 0, 0.75, and 1.5 and to a scattering angle of 180° as observed from a lidar. A wide range of effective radii falls into the same α_L category unresolved by the CALIPSO two wavelengths. It is better resolved by the MODIS wide spectral range, though the partial disorganization of the values of the effective radius for $\alpha_L = 0$ and to a smaller extend for $\alpha_L = 0.75$ shows also the limitations of the MODIS information content. The information on the aerosol size distribution that can be derived from MODIS depends also on the scattering angle Θ [19]. However, we shall show that integration of MODIS and the lidar data can overcome even this limitation. It is concluded from Fig. 1 that the use of the two lidar wavelengths can provide a first separation between modes and that the MODIS 2.1 μm can be used to define better the size distribution, however only for the entire atmospheric column.

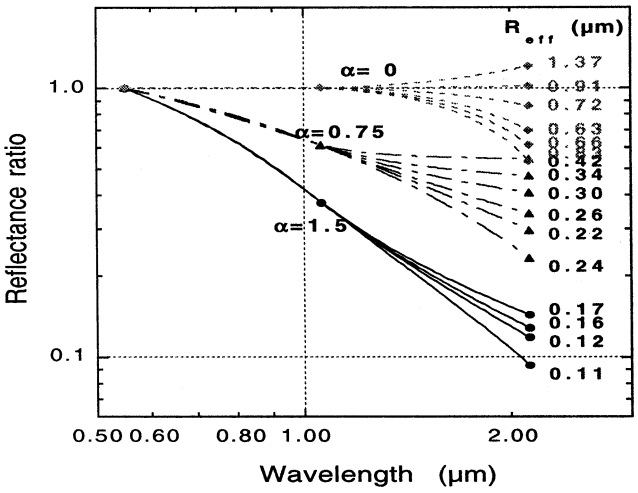

Fig. 1. Spectral normalized aerosol radiance (normalized to value of 1.0 at 0.53 μm) for a range of combinations of the aerosol fine and coarse modes that result in three specific values of the spectral slope α_L (2). The lidar two channel measurements cannot distinguish aerosol size distributions with the same α_L value. For each case the effective radius R_{eff} of the aerosol size distribution is shown. MODIS 2.1-μm channel measurements resolves the differences among the different aerosol size distributions for $\alpha_L \geq 0.75$, but not for $\alpha_L = 0$.

III. Inversion Scheme

The examples in Table I and Fig. 1 serve the basis for the algorithm developed in the Appendix and described by the flowchart of Fig. 2. From mathematical point of view, inversion of the integrated MODIS + CALIPSO lidar data still allows for many very different solutions. However, in nature, not all of these solutions occur. The chosen aerosol sizes, with associated refractive indexes, shown in Table II, do represent a simplification. They avoid mathematical solutions for effective radii around 0.5 μm, that occur in nature only for clay particles that accompany in small quantities larger dust particles [28] and aged stratospheric aerosol that is sized just in between the fine and coarse modes [29]. The result is a combination of four possible fine modes and five possible coarse modes that were selected to be used in the inversion of the MODIS data [11], [12]. Each mode represents a given aerosol scenario, from dry smoke, to wet urban pollution, salt and dust with refractive indexes assigned accordingly. The approach was found to be very successful in the inversion of aircraft and MODIS data [12], [30]. The lidar equation is solved for successive optical thin layers using the single scattering approximation. The MODIS simulations are done using full radiative transfer codes of Dave and Gazdag [31] and Ahmad and Fraser [32].

Inversion of the lidar and MODIS data is performed in two steps. First we invert the two spectral channel data of the lidar alone for all the possible combinations of the four fine and five coarse modes defined in Table II. The four fine modes include effective radius, R_{eff}, varying from 0.10–0.25 μm in step of 0.05 μm and five coarse modes, three for salt and two for dust with varying effective radii from 1–2.5 μm. Refractive indexes are selected to fit the size of each mode, assuming that larger fine mode corresponds to higher relative humidity and smaller refractive index. Table II also gives, for spherical particles, the lidar backscattering to extinction ratio, BER $= \omega_o P(180°)/4\pi$, calculated for each of the nine modes, to be used for the lidar

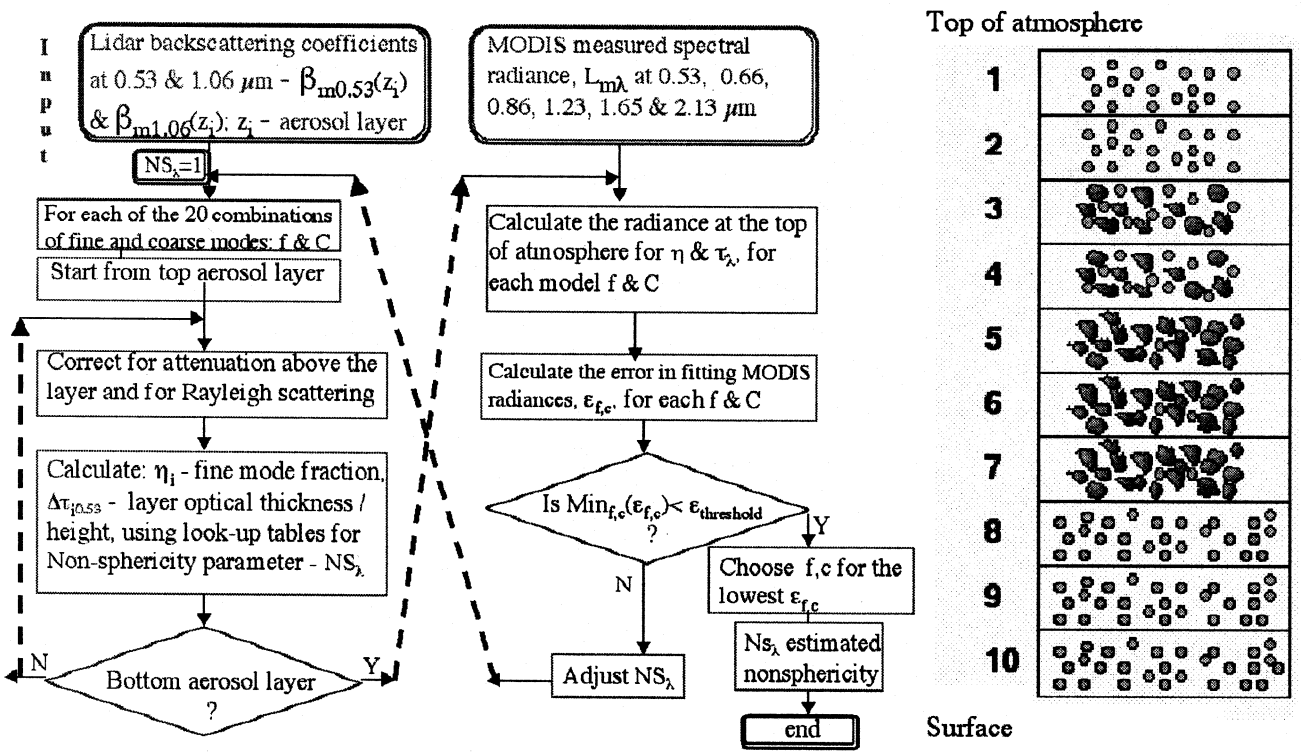

Fig. 2. Flowchart of simultaneous inversion of two wavelength lidar backscattering coefficient (e.g., from CALIPSO) and spectral passive measurements (e.g., from MODIS) over glint-free ocean. (Top left) For spherical aerosol (NS = 1) and each combination of one fine "f" and one coarse "C" modes, starting from the top aerosol layer down to the surface, derive the layer extinction, $\sigma_{0.53}$ and the fraction of fine mode, η, from the lidar backscattering coefficients, corrected for attenuation and Rayleigh scattering. (Top center) Compute the spectral radiance at the top of atmosphere and compare it with MODIS measurements. If the lowest error $\mathrm{Min}(\varepsilon_{f,c})$ for any of the f, C combinations is not smaller than a threshold value $\varepsilon_{\mathrm{threshold}}$ of about 4%, adjust NS and try again till reaching a minimum. The solution is an atmosphere characterized throughout by a specific fine and coarse modes, by vertically varying concentrations of the fine and coarse modes and by nonsphericity effect, NS, on the coarse-mode phase function at 180°. (Right) Schematic representations of an atmosphere with ten layers, with fine spherical aerosol of fixed size, nonspherical coarse aerosol of fixed size and varying vertical distributions.

TABLE II

AEROSOL MODELS FOR THE FINE AND COARSE MODES USED TO RETRIEVE THE AEROSOL PROPERTIES FROM THE INTEGRATED CALIPSO LIDAR AND MODIS DATASETS. R_g AND σ ARE THE MEDIAN RADIUS AND STANDARD DEVIATION OF THE LOG-NORMAL SIZE DISTRIBUTION. R_{eff} IS THE EFFECTIVE RADIUS OF THE DISTRIBUTION: $R_{\mathrm{eff}} = R_g \exp(2.5\sigma^2)$, AND ω_o IS THE SINGLE SCATTERING ALBEDO. THE VALUE OF THE BACKSCATTERING-TO-EXTINCTION RATIO (BER) [BER $= \omega_o P(180)/(4\pi)$] IS ALSO GIVEN. NOTE THAT THE LIDAR RATIO S IS DEFINED AS $S = 1/\mathrm{BER}$

fine particles:

	λ=0.55--0.86μm	λ=1.24μm	λ=1.64μm	λ=2.13μm	R_g μm	σ	R_{eff} μm	ω_o at 0.55 μm	BER at 0.55 μm (sr^{-1})	Comments
1	1.45-0.0035i	1.45-0.0035i	1.43-0.01i	1.40-0.005i	0.07	0.40	0.10	0.97	0.022	Small fine
2	1.45-0.0035I	1.45-0.0035i	1.43-0.01i	1.40-0.005i	0.06	0.60	0.15	0.98	0.016	Intermediate fine
3	1.40-0.0020I	1.40-0.0020i	1.39-0.005i	1.36-0.003i	0.08	0.60	0.20	0.99	0.013	Wet large fine
4	1.40-0.0020i	1.40-0.0020i	1.39-0.005i	1.36-0.003i	0.10	0.60	0.25	0.99	0.013	Wetter large fine

coarse particles:

	λ=0.55--0.86μm	λ=1.24μm	λ=1.64μm	λ=2.13μm	R_g μm	σ	R_{eff} μm	ω_o at 0.55 μm	BER at 0.55 μm (sr^{-1})	comments
5	1.45-0.0035i	1.45-0.0035i	1.43-0.0035i	1.43-0.0035i	0.40	0.60	0.98	0.94	0.035	Wet Sea salt type
6	1.45-0.0035i	1.45-0.0035i	1.43-0.0035i	1.43-0.0035i	0.60	0.60	1.48	0.90	0.035	Wet Sea salt type
7	1.45-0.0035i	1.45-0.0035i	1.43-0.0035i	1.43-0.0035i	0.80	0.60	1.98	0.88	0.032	Wet Sea salt type
8	1.53-0.001i	1.46-0.000i	1.46-0.001i	1.46-0.000i	0.60	0.60	1.48	0.97	0.076	Dust-like type
9	1.53-0.001i	1.46-0.000i	1.46-0.001i	1.46-0.000i	0.50	0.80	2.50	0.95	0.073	Dust-like type

data inversion. To obtain a unique solution, we assume that the atmospheric column is composed of only one fine aerosol mode, and one coarse mode with fixed particle size but varying concentrations as a function of height. For each of the nine models, the particle size distribution and refractive indexes are defined in Table II. What is left for the inversion scheme is to find the extinction coefficient of the fine and coarse modes so that they fit the two lidar measured backscattering coefficients. Since we use calibrated lidar data, the inversion is well defined and proceeds using simple algebraic formulation that map the two lidar measurements to the two aerosol extinctions. In other words, for a given combination of a fine (out of four) and a coarse aerosol

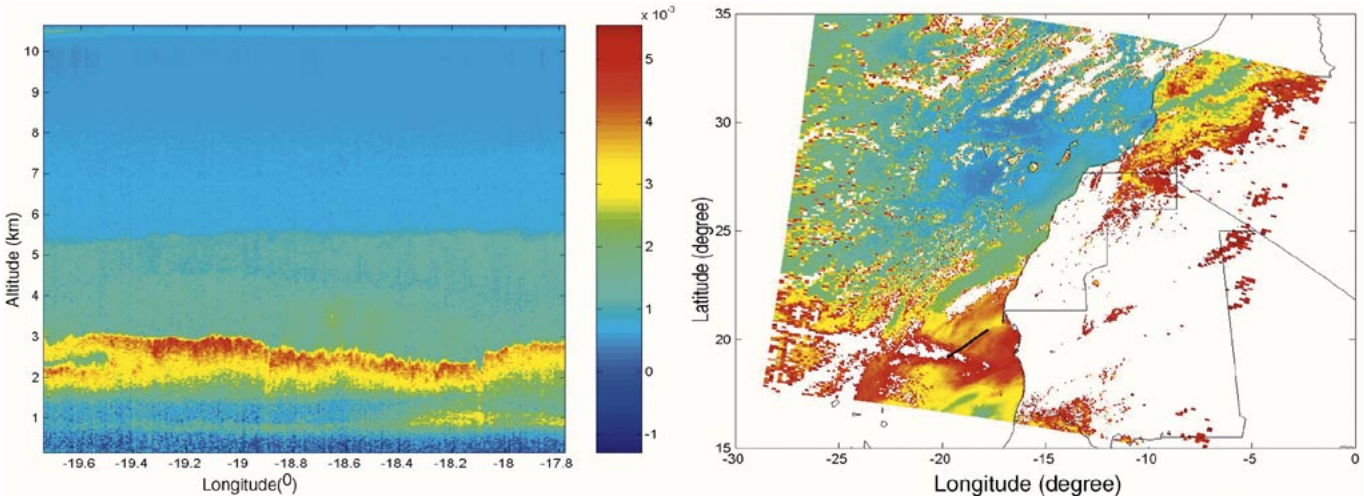

(a) (b)

Fig. 3. (a) Lidar returns at 0.53 μm as a function of height (kilometers) and longitude (°), showing the presence of dust at 2–3-km altitude. The lidar flew at 10.5-km altitude. (b) The MODIS image of the derived aerosol optical thickness is shown. Red colors correspond to high aerosol concentration and blue colors to low. The lidar path is shown in the MODIS image by black line.

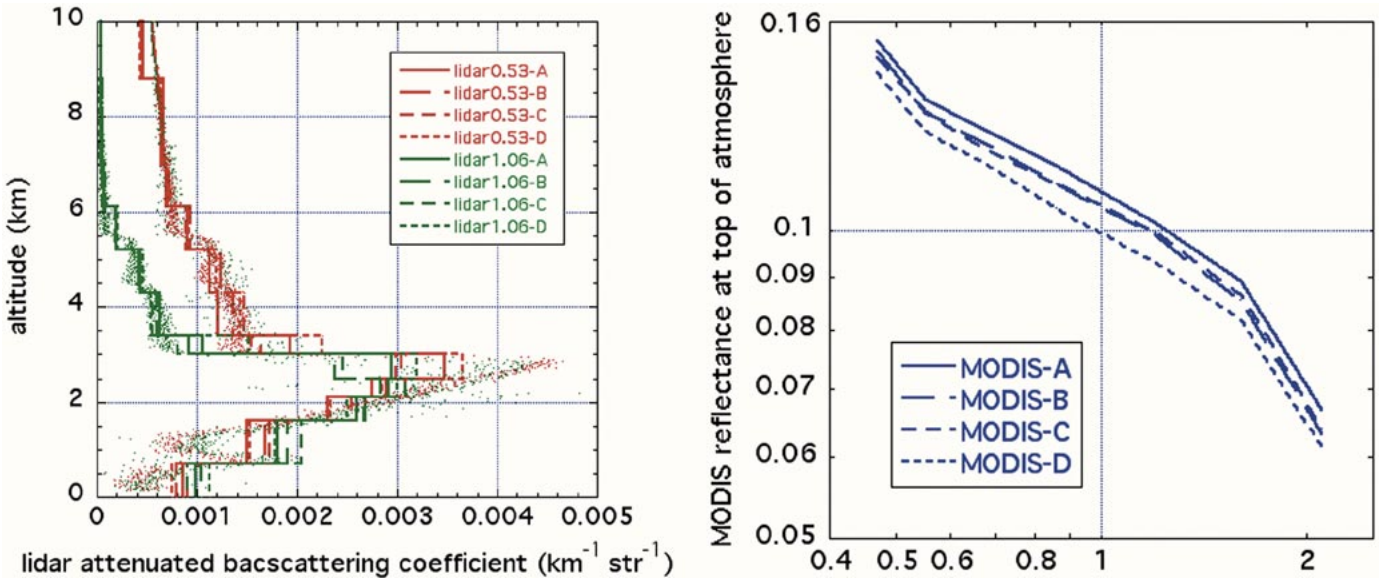

(a) (b)

Fig. 4. Input to the inversion of the aerosol profiles. (a) Four consequent profiles (from A to D) of the attenuated lidar backscattering coefficient at 0.53 μm (green) and 1.06 μm (red). The measured lidar returns, integrated on 15-m altitude are given by dots. The data were averaged into 12 nonequal steps shown by the four green and four red lines. (b) Four corresponding MODIS spectral reflectances (from A to D) measured over the ocean at the top of the atmosphere, outside the ocean glint. The letters A, B, C, and D show the corresponding lidar and MODIS measurements.

(out of five) modes, the ambiguity in the inversion of the lidar data is removed and a unique profile of the optical thickness of the fine and coarse modes is derived from the lidar data.

Note that to obtain a unique solution for each of the 20 (4×5) mode combinations, it is assumed that the size of the particles in each of these modes does not vary with altitude, contrary to what one may expect from altitude variations of the relative humidity or sedimentation of large particles. The concentrations of each mode is allowed to vary with altitude independently of each other, based on the lidar 2 wavelength signal. We tested the effect of this hypothesis by inverting simulated data with accumulation mode varying in size from 0.15 μm near the surface to 0.25 μm at 2-km height. The resultant inversion gave best results for the intermediate size of 0.2 μm. To find the variation of the accumulation mode with height, the fraction of coarse mode as function of height has to be known from other sources. This may be possible in principle using the depolarization as a measure of the ratio of spherical accumulation mode to nonspherical coarse mode, but requires very accurate measurements of the depolarization, and is not discussed in this paper.

In the second step, the retrieved aerosol profiles for each of the 20 combinations are used to calculate 20 sets of MODIS spectral reflectances. Each of the 20 cases fits precisely the lidar data and the decision, which of the combinations is the proper one, is left to the MODIS measurements alone. The combination of a fine and a coarse mode that fits the MODIS measured spectral reflectances with minimal error is the "winning" combination.

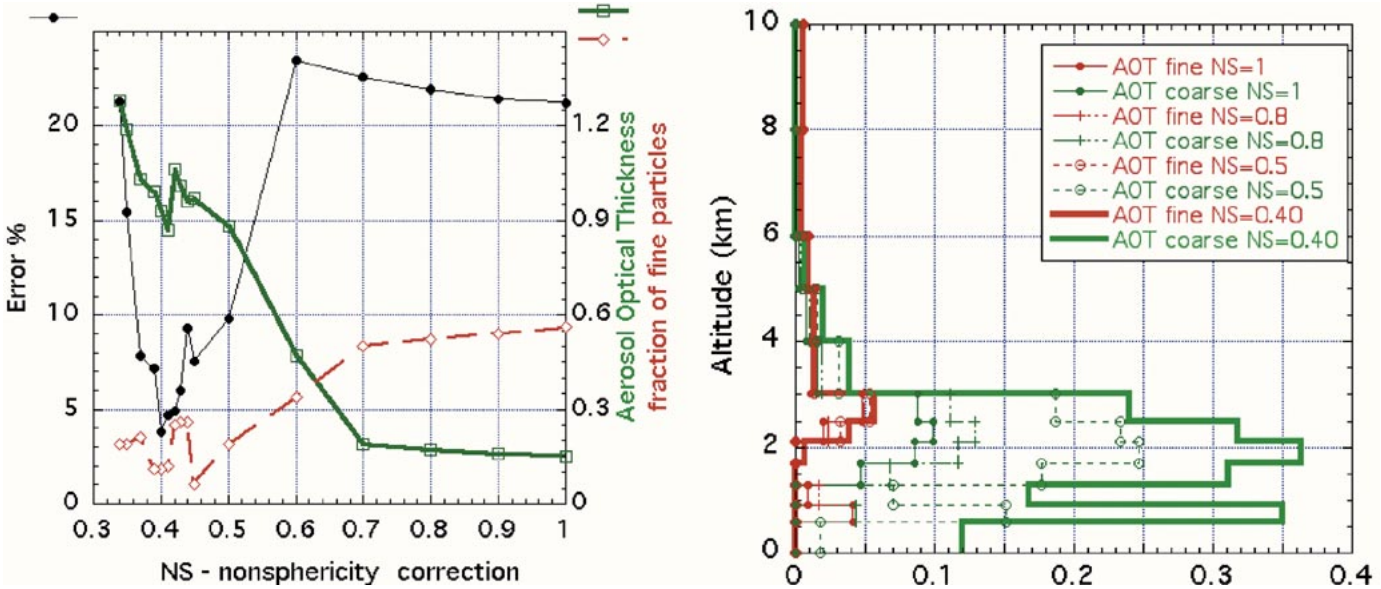

(a) (b)

Fig. 5. Sensitivity of the inversion of lidar+MODIS data to the nonsphericity parameter—NS. Here the same nonsphericity was chosen for the two lidar wavelengths. In the inversion process, the lidar backscattering phase function associated with coarse particles was multiplied by NS to account for the effect of aerosol nonsphericity on the phase function at 180°. (a) The error in fitting the MODIS spectral reflectance (thin solid black line), and the aerosol optical thickness (thick solid green line) and fraction of fine particles contribution to the optical thickness (red dashed line) that resulted from the inversion. For NS $= 0.40$, there is on both sides a sharp decline in the error. For this value, the fraction contribution of the fine mode is small (11%) as expected for the dust episode. (b) Profiles of the fine and coarse aerosol for several values of NS.

IV. Application to SHADE Data

The integrated CALIPSO-MODIS algorithm is applied to LEANDRE 1 lidar data onboard the French Mystère-20 research aircraft during the SHADE experiment off the West Africa coast [see Fig. 3(b)] over the Northeastern Tropical Atlantic. The LEANDRE 1 system offers the same observational capability that the CALIPSO lidar (two channels at 0.53 and 1.06 μm and depolarization at 0.53 μm). We used here coincidental lidar and MODIS data within 20 min on September 26, 2000. Observations were acquired between the West coast of Africa and the Cape Verde archipelago. This location is well-known to be the main area of dust transport over the tropical Atlantic [33]. The atmospheric aerosol is dominated by dust from the Sahara [34]. During summer time, the African dust is transported across the Atlantic in a dry and warm stable layer, the so-called Saharan air layer (SAL), located between 1.5 and 6 km in altitude [35]. A conceptual model for the SAL has been proposed and validated by *Karyampudi et al.* [36]. This analysis shows that such a kind of dust transport occurs in September. During winter time, a low altitude transport of dust in the trade winds may prevail [37].

The lidar attenuated backscattering coefficient at 0.53 μm and the corresponding image of the MODIS-derived optical thickness are shown in Fig. 3. They show the three dimensional structure of the dust layer. Examples of the MODIS spectral reflectance and the lidar profiles of the attenuated backscattering coefficient at 0.53 and 1.06 μm are plotted in Fig. 4. The lidar backscattering attenuated coefficient is reported in 15-m vertical resolution steps. The main dust layer is seen to extend up to 3 km in altitude, although the whole dust outbreak is seen to reach an upper altitude of 7–8 km. We averaged the data in nonequal steps based on the strength of the lidar signal, to optimize qualitatively the lidar signal vs. the vertical resolution and structure. The averaged functions are shown by lines in the figure. The steps capture the main features of the lidar return signal, for the dust at 2–3 km and for the top of the marine boundary layer at 0.8 km.

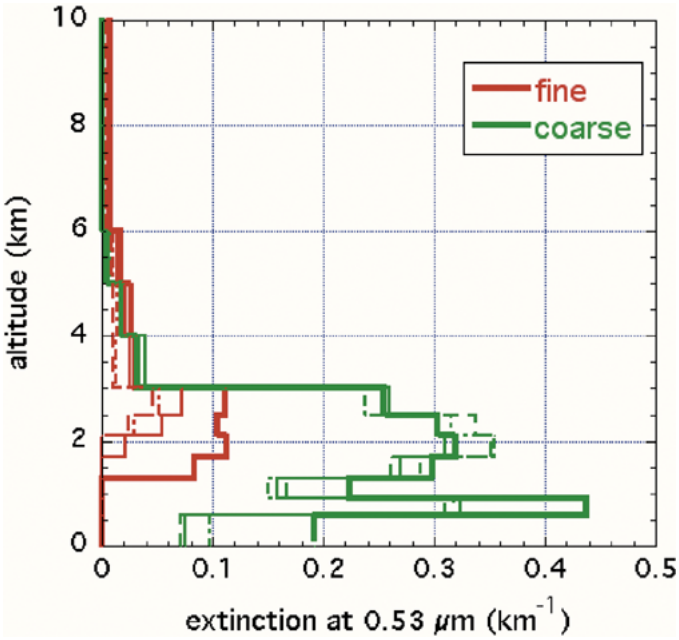

Fig. 6. Results of inversion of the lidar profiles and MODIS spectra of Fig. 4. The different line types identify results of inversion of the four cases given in Fig. 4. Note that the maximum extinction occurs in lower altitude than the maximum backscattering coefficient due to its attenuation by the aerosol above the given layer.

V. Dust Nonsphericity

To invert dust data using LEANDRE 1 and MODIS measurements we have to account for the effects of nonsphericity on the scattering phase function of dust. The MODIS data for the dust layer are for scattering angle of $\sim$135° while the lidar return is of course for the scattering angle of 180°. For 135° scattering angle dust nonsphericity has a small impact on the scattering phase function [38], much smaller than at 180°. Further multiple scattering for the high dust loading of SHADE, reduces the effect of nonsphericity on the MODIS measurements but not as much on the lidar measurements. Multiple scattering impact on the aircraft lidar data is expected to be of the order of a few per-cent for the small distance between the aircraft and aerosol ($<$10 km). It is, however, expected to be somewhat larger for CALIPSO spaceborne measurements [39].

To account for the nonsphericity effect on the lidar returns, we introduced a nonsphericity parameter, NS_λ, that reduces the value of the lidar spherical phase function at $\lambda = 0.53\mu$m and 1.06 μm for 180° scattering angle. The parameter NS_λ is determined for each wavelength by the following iterative procedure (see the flowchart in Fig. 2 and the plots in Fig. 5). First the lidar and MODIS data are inverted without the effect of nonsphericity ($\mathrm{NS}_\lambda = 1.0$). The best solution, illustrated in Fig. 5, fitted the MODIS radiances with an error ε [see (A14) in the Appendix] of 21%. Since the lidar calibration errors are expected to be smaller than 5%, and MODIS calibration errors smaller than 2%, the large error of 21% is an indicator that the scattering phase function used in the lidar inversion is not appropriate and that the retrieved optical thickness of 0.15 and fraction of fine particles of 0.55 are not correct. The iterative scheme, then tries different values of NS_λ, inverting the measurements for each set of values, and finding that $\mathrm{NS}_{0.53} = 0.41$ and $\mathrm{NS}_{1.06} = 0.40$ at 0.53 and 1.06 μm, respectively, give the best results with an error in fitting the MODIS radiances of $\varepsilon = 3.8\%$ and corresponding optical thickness of 0.9 and fraction of fine particles of 0.2 (see Fig. 5). The validity of the nonsphericity factor NS_λ is further confirmed by the fact that values of NS_λ retrieved at both wavelengths are very close one to another, as expected for dust particles (2-μm effective diameter) that are larger than the wavelength (0.53–1.06 μm). The values of NS$\sim$0.41, 0.40 are similar to calculations of the ratio of phase function of spheroids to spheres for size parameter $X(X = 2\pi r/\lambda)$ of 15 to 25 that corresponds to dust with effective radius of 2 μm [40]. For NS < 0.40 or NS > 0.45 the error in fitting the MODIS radiances using the lidar retrievals is too large ($\varepsilon > 7\%$) to make these values credible. Fig. 5(b) shows the profiles of the extinction coefficient of the fine and coarse particles for the optimum solution (NS $= 0.40$) and for some other values of NS.

Inversion products of the lidar and MODIS data of Fig. 4 are shown in Fig. 6. Note that correction of the attenuation of the backscattering function by the aerosol layers in the inversion process shifts the maximum extinction of the coarse mode from an altitude of 2–3 km. The dust layer is composed mainly of coarse particles ($R_{\mathrm{eff}} = 1.5\,\mu$m), but accompanied by 10% to 20% of fine particles ($R_{\mathrm{eff}} = 0.1\,\mu$m). At 4–6 km, there are more fine particles than coarse particles according to the inversion. The layer at the top of the boundary layer was determined to be composed of coarse particles, probably sea salt. Note that some of these results may be still influenced by the lack of nonspherical model in the MODIS lookup table. The lidar ratio, S, derived in this inversion at both wavelengths is $S = 63 \pm 6$ sr, which gives a value of the backscattering to extinction ratio of $\mathrm{BER} = \omega_o P(180°)/4\pi = 0.016\ \mathrm{sr}^{-1}$. It has to be compared to the value of $S = 30$ sr ($\mathrm{BER} = 0.035\ \mathrm{sr}^{-1}$ [41]) when nonsphericity is not considered. Our value is in good agreement with the one derived from lidar data analysis and with values recently found from ground-based Raman lidar measurements [42].

Can the lower BER value result from other processes beside nonsphericity? An uncertainty in the value of BER of 10% to 15% can be associated with the following:

- uncertainty in dust absorption ($\pm$3% at 0.53 μm and $\pm$1% at 1.06 μm—[43], [16]),
- uncertainty in the MODIS and lidar calibration ($\pm$5%),
- uncertainty in the nonsphericity effect on the MODIS spectral radiances ($\pm$10%).

Therefore, the reduction in the BER value by more than 50% cannot be explained and should be associated mainly with the effect of dust nonsphericity on the phase function at 180°.

VI. Sensitivity to Calibration Errors and Noise

MODIS retrievals over the oceans are informative down to optical thickness of 0.1 at 0.55 μm [11], [12], [30]. Above this optical thickness the MODIS data are expected to be useful in the lidar inversion. What is the sensitivity of the inversion to calibration errors and noise in the lidar data? In the following we discuss the sensitivity with the help of the dust data from the SHADE experiment, but first we show some details of the fitting process. In Fig. 7(a), we show five representative solutions out of the 20 combinations, Two solutions (solid and dotted green lines) have similar fitting error of 4% to 5%, but somewhat different aerosol characteristics, i.e., effective radiuses, optical thickness and ratio. This shows some of the inherent uncertainty in the inversion. The other solutions deviate significantly from the model and have significantly higher fitting errors of 12% to 30%.

It is expected that the satellite lidar data will be more noisy than the aircraft lidar, due to the larger distance of 700 km versus 8 km from the dust layer. Noise in the lidar system may result also in a bias, or error in the absolute lidar calibration for a given profile. We tested several cases with calibration errors in the two channels of 5% and 10% [Fig. 7(b)]. Calibration error of 5% in both channels introduces an error of 20% in the column optical thickness (for example a total optical depth of 1.07 is retrieved instead of 0.86 for a calibration bias of +5%). However, the fit to MODIS data had in this case an unrealistic high error of $\varepsilon = 9\%$. ε is thus significantly degraded due to inconsistency between the lidar and MODIS data, due to the calibration errors. Double calibration error (10%) doubles the error in the optical thickness and farther increases the error in fitting the MODIS data to 16%. ε is sensitive not only to calibration errors but also to effects of aerosol nonsphericity. However, analysis of the MODIS and

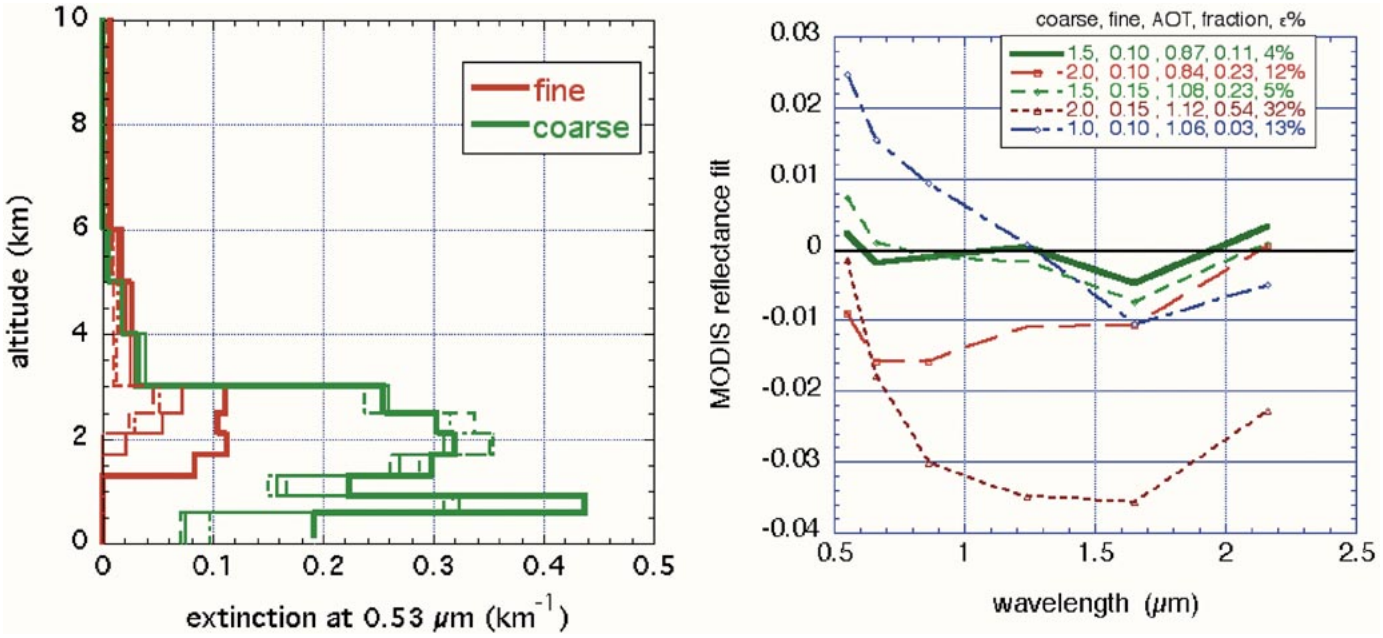

(a) (b)

Fig. 7. (a) Spectra of the difference between the MODIS measured spectral reflectance and the derived solution for five representative model combinations for the same inversion. For each solution we show in (a) R_{eff} of the coarse and fine modes (μm), the optical thickness (AOT), fraction of the AOT due to the fine mode, and the error in fitting the MODIS-measured spectral reflectances. (b) Sensitivity of the inversion of the aerosol profiles to errors in lidar calibration of 5% to 10% in each or both of the channels as indicated. Profiles of the extinction coefficients of the fine (red) and coarse (green) aerosol models are shown. The heavy line shows the solution with no additional errors. The values of the column optical thickness of the fine (τ_f) and coarse (τ_c) aerosols are given in the figure.

lidar data can be used to improve the lidar calibration or to find the aerosol nonsphericity parameter NS but not both.

Introduction of noise to the lidar data has a much smaller effect on the inversion than systematic calibration errors. We added random errors to the lidar backscattering profile using the transformation

$$\beta_\lambda \rightarrow \beta_\lambda(1 + rC_N/100\%)$$

where r is a random number between -1 and $+1$ and C_N is the magnitude of the noise. We decided to consider a noise of 10% at $\lambda = 0.53\,\mu$m and 20% at $\lambda = 1.06\,\mu$m. Profiles of the inverted extinction coefficient (Fig. 8) show that the noise did not change the fundamental properties of the derived aerosol layer. The differences are larger for the fine mode due to its small contribution to the optical thickness in this case. Addition of the noise did not have a systematic effect on the column properties. It changed the column optical thickness at 0.53 μm from 0.87 to 0.85 ± 0.1. The fraction of the fine mode in the optical thickness increased from 0.11 to 0.14 ± 0.08. The inversion process identified the same modes of the fine and coarse particles 80% of the time. A histogram of the optical thicknesses derived in 46 calculations with random noise is shown in Fig. 9.

It is thus expected that increasing the noise level will degrade accuracy of the retrieval in a statistical sense. As a matter of fact, the relative error cannot be considered as constant over the whole vertical profiles but more likely depending on the lidar signal and background noise [44]. Adjusting vertical and horizontal resolution as a function of extinction may somewhat allow to compensate for this dependence and get closer to the hypothesis used here. Such an averaging is allowed by the rather

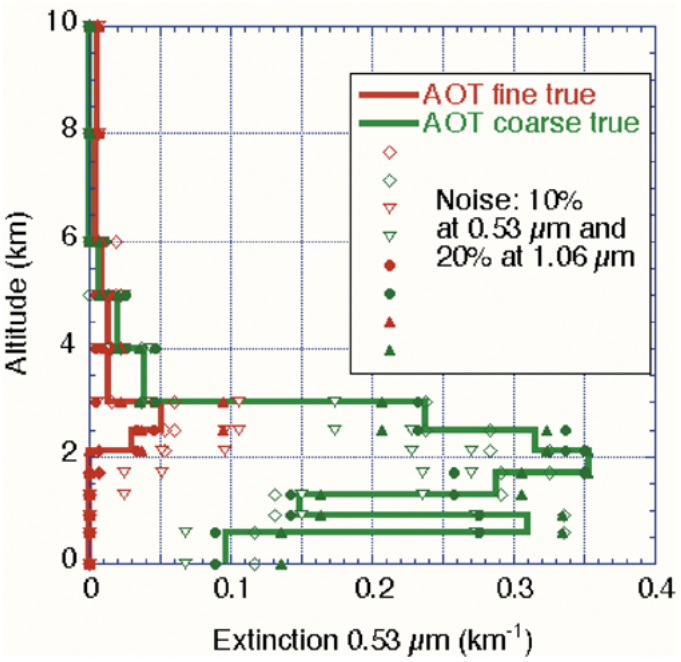

Fig. 8. Profiles of the extinction coefficient obtained for the original data with no additional noise (solid thick lines) and for four cases where random noise was added in the backscattering coefficient of 10% at 0.53 μm and 20% at 1.06 μm (symbols). Fine mode is shown by red and coarse mode by green.

large coherence scale of aerosol patterns. Anderson *et al.* [45] indicated coherence patterns smaller than 200 km. Near aerosol sources, aerosol variation is expected to be on smaller scales; therefore, averaging of 10–50 km of the lidar measurements along track over the ocean is recommended.

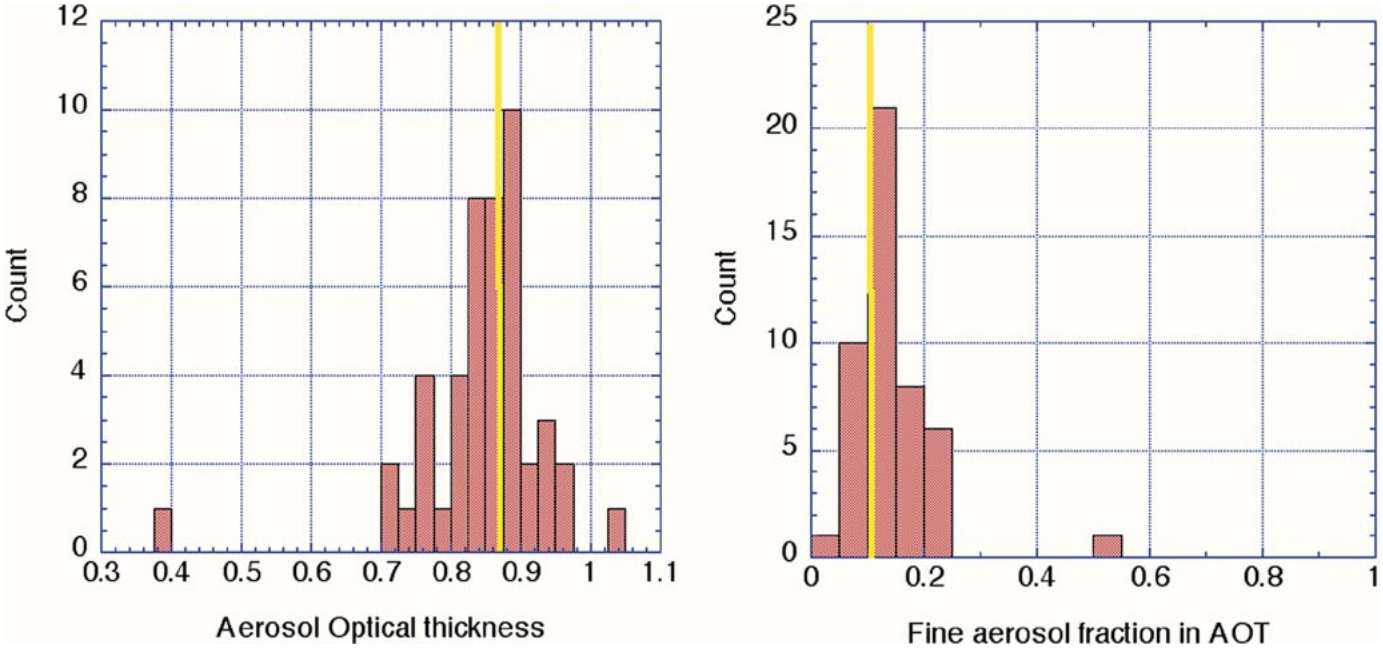

(a) (b)

Fig. 9. Histogram of the (a) column aerosol optical thickness and (b) fine aerosol fraction obtained in the presence of random noise in the backscattering coefficient of 10% at 0.53 μm and 20% at 1.06 μm. The yellow line is the solution without the noise.

VII. Conclusion

Combined inversion of the MODIS spectral radiances with the CALIPSO 2 wavelength profiles of the attenuated backscattering coefficients takes advantage of the wide MODIS spectral range and the vertical profile information in the lidar data. A new inversion code was developed that applies to MODIS and 2 wavelength lidar data acquired during daytime over glint-free oceans. The inversion chooses one fine and one coarse mode, out of a lookup table and produces separate vertical profiles of the fine and coarse modes. In cases where the size of the fine or coarse modes vary with altitude, the inversion was found to choose the average size to represent the column. The inversion was shown to be sensitive to the data quality. Introduction of calibration errors into the lidar data or the presence of nonsphericity is not compensated by a different aerosol profile but rather results in large and unacceptable retrieval errors. This feature can be used to improve the calibration of the lidar or the MODIS instrument, or improve the aerosol model.

Application to the SHADE data over heavy dust from Africa resulted as expected in profile of mainly dust, in agreement with *in situ* measurements from previous day [20]. Due to the excellent MODIS and aircraft lidar calibrations (maximal errors of 2% and 5%, respectively), the procedure was used to derive the effect of dust nonsphericity on the dust scattering phase function at 180°. Nonsphericity reduced the value of the phase function to 0.41 from its Mie value, resulting in extinction-to-backscattering ratio of BER $= 0.016$ sr^{-1}, or lidar ratio, S, at 0.53 μm of $S = 63 \pm 6$ sr, and $S = 57 \pm 6$ sr at1.06 μm.

Inversion of the lidar data could be done using alternative techniques, e.g., using the MODIS spectral optical thickness to restrict the inversion and define the lidar ratio (similar to the inversion of ground-based lidars using sunphotometers) or using an intermediate technique [20], where the MODIS optical thickness is used first to correct for the attenuation of the lidar signal through the atmosphere, for each combination of fine and coarse aerosols, and the MODIS spectral data used later to define the fine and coarse modes. There are advantages in these techniques by means of speed, reduced MODIS data volume (if only optical thickness is used), or stability against calibration and nonsphericity errors. The present technique has the advantage that the inverted optical thickness, fraction of fine aerosol, and the size of the fine and coarse aerosol are defined using a combination of the MODIS and lidar data, taking advantage of their different sensitivity to the aerosol optical thickness and phase function. This additional sensitivity was used here to estimate the effect of dust nonsphericity on the lidar ratio.

Further improvement in the analysis is expected from additional synergism. The PARASOL mission with a POLDER instrument onboard will be part of the same train as AQUA and CALIPSO satellites. It will take passive measurements of the two-dimensional polarized radiation field in five spectral channels in the 0.44–0.91-μm range and for wide range of view zenith angles and all azimuth directions [46]. This information when integrated into the MODIS+CALIPSO data will further constrain the inversion. POLDER also measures the light polarization and CALIPSO measures the depolarization profile, both helping to distinguish spherical particles from nonspherical ones and in case of POLDER adding sensitivity to the particle refractive index not derived from the MODIS data. Polarization is also expected to constrain better the size of the fine mode.

Over the land, the present inversion is not possible; however, MODIS data can be used to restrict the lidar inversion by specifying the total column optical thickness (see [20]). If MODIS derives also the fraction of the optical thickness due to the fine aerosol over the land, this product is presently not very accurate. Improvement in the MODIS derivation over the land, or inclusion of the POLDER observations of the fine aerosol [47]

may allow separation between the fine and coarse aerosol profiles also over land surfaces.

APPENDIX
INVERSION SCHEME

This Appendix describes the simultaneous inversion of the MODIS spectral radiances in the 0.55–2.13-μm range together with the CALIPSO two-wavelength (0.53 and 1.06 μm) lidar. The total particle backscatter β_λ at wavelength λ is defined as the product between the aerosol normalized backscatter phase function and the aerosol scattering coefficient. This also applies to molecular scattering, where the normalized backscatter phase function for molecules is constant and equal to $3/8\pi$. For a given optically thin layer of optical thickness $\Delta\tau_\lambda$ and height ΔH, the total particle backscatter is defined by [48], [49]

$$\beta_\lambda = C_L \omega_\lambda P_\lambda(180) \Delta\sigma_\lambda \ \left(\text{str}^{-1}\text{km}^{-1}\right) \tag{A1}$$

where C_L is a constant that defines the lidar properties, and $\Delta\sigma_\lambda$ is the extinction coefficient, given by

$$\sigma_\lambda = \Delta\tau_\lambda / \Delta H \ \left(\text{km}^{-1}\right). \tag{A2}$$

In the inversion, we assume that the lidar equation can be inverted using the single scattering approximation for each of the layers. For the MODIS data a lookup table, generated using full radiative transfer calculations of the Dave and Gazdag [31] and Ahmad and Fraser [32] code is used.

Step 1: Inversion of the CALIPSO Data

For each combination of a fine "f" and a coarse "C" modes, the two wavelength backscattering coefficients measured by the lidar for layer "i" are inverted to give the layer extinction coefficient $\Delta\sigma_\lambda$ and the fraction of the extinction due to the fine aerosol. The layers do not have to be of the same optical or geometrical thickness, and the top layer does not have to be at the top of the atmosphere. However, no significant amount of aerosol should be present above the top layer. In this paper, the top layer is between 9 and 10 km above the surface, just under the aircraft. For space application, the top layer can include the stratosphere.

The inversion starts from the top aerosol layer $(i = 1)$. For each layer, the measurements are the attenuated backscattering coefficients by the aerosol and molecules in the layers above. Therefore, for layer "i," the measured attenuated backscattering coefficients $\beta'_{m\lambda,i}$ have to be corrected first for the attenuation by aerosol optical thickness of layers 1 through $i-1$, and for the attenuation by Rayleigh molecular scattering

$$\tau_{\lambda,\,i-1} = \Delta\tau_{\lambda,1} + \cdots + \Delta\tau_{\lambda,i-1} + \tau_{R\lambda,i-1} \tag{A3}$$

where $\tau_{R\lambda,i-1}$ is the Rayleigh optical thickness from top of the atmosphere down to layer i. The measured attenuated backscattering coefficient for the layer i, $\beta_{m\lambda,i}$ is related to the nonattenuated aerosol backscattering coefficient in the layer $\beta'_{m\lambda,i}$ by

$$\beta_{m\lambda,i} = [\beta'_{m\lambda,i} + \beta_{R\lambda,i}] \exp(-2\tau_{\lambda,i-1}). \tag{A4}$$

Therefore, the correction for attenuation is

$$\beta'_{m\lambda,i} = \beta_{m\lambda,i} \exp\left(2\tau_{\lambda,i-1}\right) - \beta_{R\lambda,i}. \tag{A5}$$

The corrected backscattering are suitable for the actual inversion, from $\beta'_{m0.53,i}$ and $\beta'_{m1.06,i}$ to the fraction of the fine aerosol in the extinction, η_i, and the extinction itself, $\sigma_{0.53,i}$. The spectral ratio ξ_{mi}

$$\xi_{m,i} = \beta'_{m1.06,i} / \beta'_{m0.53,i} \tag{A6}$$

is used to determine η_i. We define a normalized backscattering coefficient that does not depend on the aerosol extinction or layer height but is sensitive to the aerosol size $\beta^*_\lambda = \beta'_\lambda / \Delta\sigma_{0.53}$, where $\Delta\sigma_{0.53}$ is the extinction coefficient at 0.53 μm

$$\beta^*_{\lambda,i} = C_L \omega_{\lambda,i} P_{\lambda,i}(180) \sigma^*_{\lambda,i} = \beta'_{m\lambda,i} / \sigma_{0.53} \tag{A7}$$

where $\sigma^*_{1.06} = \sigma_{1.06}/\sigma_{0.53}$ and $\sigma^*_{0.53} = 1$.

Once the aerosol model is determined by the inversion process, the phase function and the single scattering albedo can be recomputed and used together with the backscattering coefficients at $\lambda = 0.53$ to derive the optical thickness.

The aerosol backscattering coefficients $\beta'_{m\lambda,i}$ are combined from a fraction η_i of fine-mode backscattering and fraction $(1-\eta_i)$ of coarse-mode backscattering

$$\beta'_{m\lambda,i} = \eta_i \beta'_{\lambda,f} + (1-\eta_i)\beta'_{\lambda,C}. \tag{A8}$$

From (A6) and (A8), we express the spectral ratio $\xi_{m,i}$ as a function of η_i

$$\xi_{m,i} = \frac{\left[\eta_i \beta'_{1.06,f} + (1-\eta_i)\beta'_{1.06,\,C}\right]}{\left[\eta_i \beta'_{0.53,f} + (1-\eta_i)\beta'_{0.53,C}\right]}. \tag{A9}$$

Therefore

$$\eta_i = \frac{\left[\beta^*_{1.06,C} - \xi_{mi}\beta^*_{0.53,C}\right]}{\left[\xi_{mi}\beta^*_{0.53,f} - \xi_{mi}\beta^*_{0.53,C} - \beta^*_{1.06,f} + \beta^*_{0.53,C}\right]}. \tag{A10}$$

Note that the only dependence of η_i on the specific properties of level i are through ξ_{mi}, since the functions β^* are predetermined for the whole aerosol column. The expression for the extinction $\sigma_{0.53,i}$ is then derived from (A7) and (A8)

$$\sigma_{0.53,i} = \frac{\beta_{m0.53,i}}{\left[\beta^*_{0.53,f}\eta_i + (1-\eta_i)\beta^*_{0.53,C}\right]}. \tag{A11}$$

Let us mention that not every mode combination will give a physical solution. Unphysical solutions will be reflected in values of η_i larger than 1.0 or negative. If the value of η_i for any layer with significant aerosol concentration $(\Delta\tau_{0.53} > 0.02)$ is $\eta_i > 1.3$ or $\eta_i < -0.3$, the solution for this mode combination is void; otherwise it is rounded to 1.0 and 0.0, respectively.

Step 2: Use of MODIS Spectral Data

Let us first remind that we do not resolve variations in the size of the fine or coarse modes with altitude. Inversion of the CALIPSO data resulted in up to 20 different combinations of fine and coarse aerosol profiles, all of them reproducing the lidar profile of the attenuated backscattering coefficient at 0.53 and 1.06 μm. That means that although the 20 combinations have different properties of the fine and/or coarse modes, it was possible to find extinction coefficients of the fine and coarse modes that fit precisely the profiles of the lidar data in the two wavelengths. In step 2, the MODIS measured spectral radiance

$L_{m\lambda\mathrm{MOD}}$ is used to choose the best solution of the lidar data between these 20. For each of the combinations of the fine "f" and coarse "C" modes, inversion resulted in $\eta_{i,f,C}$, $\sigma_{0.53,i,f,C}$, for layer "i." The column total optical thickness $\tau_{0.53,f,C}$ and the contribution of the fine mode in the entire column, $\eta_{f,C}$ is then

$$\begin{aligned}\tau_{0.53,f,C} &= \Sigma\Delta\tau_{0.53,i,f,C} = \Sigma H_i\sigma_{0.53,i,f,C}\eta_{f,C} \\ &= [\Sigma(\eta_{i,f,C}\Delta\tau_{0.53,i,f,C})]/\tau_{0.53,f,C}. \quad \text{(A12)}\end{aligned}$$

For each "f" and "C" with corresponding $\tau_{0.53,f}$ or $\tau_{0.53,C}$ and $\eta_{f,C}$ a unique MODIS spectral radiance $L_{\lambda\mathrm{MOD},f,C}$ is calculated using a radiative transfer code for modes f and C for each wavelength λ. The radiances are combined using the fraction parameter $\eta_{f,C}$ [similar to (4)]

$$L_{\lambda\mathrm{MOD},f,C} = \eta_{f,C}L_{\lambda\mathrm{MOD},f} + (1-\eta_{f,C})L_{\lambda\mathrm{MOD},C} \quad \text{(A13)}$$

and compared with the measured MODIS radiance $L_{m\lambda\mathrm{MOD}}$. An error $\varepsilon_{f,C}$ is calculated for each fine- and coarse-modes combination [11]

$$\varepsilon_{f,C} = (1/6) \cdot \left[\Sigma_\lambda(L_{\lambda\mathrm{MOD},f,C} - L_{m\lambda\mathrm{MOD}})^2/(L_{m\lambda\mathrm{MOD}})^2\right]^{0.5}. \quad \text{(A14)}$$

The minimum value of $\varepsilon_{f,C}$ determines the solution. It is used to choose the best combination "f" and "C" with corresponding profiles η_i, $\sigma_{0.53,i}$ and $\sigma_{1.06,i}$. The summation is on the six MODIS channels 0.55–2.1 μm.

Value of the minimum parameter $\varepsilon_{f,C}$ can also indicate problems in the retrievals, in particular, problems with calibration, or suitability of the look up table. In this paper, the calibration is expected to be accurate within $\pm 5\%$; however, the original values of $\varepsilon_{f,C}$ indicated errors of 15% to 20%. We were able to reduce the error in the fit by introducing a scaling factor in the coarse-mode phase function due to nonsphericity, by replacing the value of the scattering phase function at 180° from P_λ (180°) to $\mathrm{NS}_\lambda P_\lambda$ (180°), where NS_λ is the nonsphericity parameter ranging from 0 to 1.

REFERENCES

[1] Y. J. Kaufman, D. Tanré, and O. Boucher, "A satellite view of aerosols in the climate system," *Rev. Nature*, vol. 419, pp. 215–223, 2002.

[2] S. A. Twomey, M. Piepgrass, and T. L. Wolfe, "An assessment of the impact of pollution on the global albedo," *Tellus*, vol. 36B, pp. 356–366, 1984.

[3] D. Rosenfeld, "Suppression of rain and snow by urban and industrial air pollution," *Science*, vol. 287, pp. 1793–1796, 2000.

[4] G. Feingold, W. R. Cotton, S. M. Kreidenweis, and J. T. Davis, "Impact of giant cloud condensation nuclei on drizzle formation in marine stratocumulus: Implications for cloud radiative properties," *J. Atmos. Sci.*, vol. 56, pp. 4100–4117, 1999.

[5] D. Rosenfeld, R. Lahav, A. P. Khain, and M. Pinsky, "The role of sea-spray in cleansing air pollution over ocean via cloud processes," *Science*, vol. 297, pp. 1667–1670, 2002.

[6] J. E. Hansen and M. Sato, "Trends of measured climate forcing agents," in *Proc. Nat. Acad. Sci.*, vol. 98, 2001, pp. 14 778–14 783.

[7] V. Ramanathan, P. J. Crutzen, J. T. Kiehl, and D. Rosenfeld, "Atmosphere—Aerosols, climate, and the hydrological cycle," *Science*, vol. 294, pp. 2119–2124, 2001.

[8] J. V. Martins *et al.*, "1998: Effects of black carbon content, particle size, and, mixing on light absorption by aerosol particles from biomass burning in Brazil," *J. Geophys. Res.*, vol. 103, pp. 32,041–32 050, 1998.

[9] S. Menon, J. Hansen, L. Nazarenko, and Y. Luo, "Climate effects of black carbon aerosols in China and India," *Science*, vol. 297, pp. 2250–2253, 2002.

[10] J. Lelieveld *et al.*, "Global air pollution crossroads over the Mediterranean," *Science*, vol. 298, pp. 794–799, 2002.

[11] D. Tanré, Y. J. Kaufman, M. Herman, and S. Mattoo, "Remote sensing of aerosol over oceans from EOS-MODIS," *J. Geophys. Res.*, vol. 102, pp. 16 971–16 988, 1997.

[12] L. A. Remer *et al.*, "Validation of MODIS aerosol retrieval over ocean," *Geophys. Res. Lett.*, vol. 29, no. 12, 2002.

[13] W. A. Hoppel *et al.*, "Aerosol size distribution and optical properties found in the marine boundary layer over the Atlantic Ocean," *J. Geophys. Res.*, vol. 95, pp. 3659–3686, 1990.

[14] L. A. Remer and Y. J. Kaufman, "Dynamical aerosol model: Urban/industrial aerosol," *J. Geophys. Res.*, vol. 103, pp. 13 859–13 871, 1998.

[15] L. A. Remer *et al.*, "Tropical biomass burning smoke aerosol size distribution model," *J. Geophys. Res.*, vol. 103, pp. 31 879–31 892, 1998.

[16] O. Dubovik *et al.*, "Climatology of aerosol absorption and optical properties in key worldwide locations," *J. Atmos. Sci.*, vol. 59, pp. 590–608, 2002.

[17] B. N. Holben *et al.*, "AERONET—A federated instrument network and data archive for aerosol characterization," *Remote Sens. Environ.*, vol. 66, pp. 1–16, 1998.

[18] B. N. Holben *et al.*, "An emerging ground-based aerosol climatology: Aerosol optical depth from AERONET," *J. Geophys. Res.*, vol. 106, pp. 12 067–12 097, 2001.

[19] D. Tanré, M. Herman, and Y. J. Kaufman, "Information on aerosol size distribution contained in solar reflected radiances," *J. Geophys. Res.*, vol. 101, pp. 19 043–19 060, 1996.

[20] J. F. Leon, D. Tanré, J. Pelon, and Y. J. Kaufman, "Characterization of tropospheric aerosols based on active and passive remote sensing synergy," J. Geophys. Res., 2002, submitted for publication.

[21] D. Müller *et al.*, "Retrieval of physical particle properties from lidar observations of extinction and backscatter at multiple wavelengths," *Appl. Optics*, vol. 37, pp. 2260–2263, 1998.

[22] C. Bockmann, "Hybrid regularization method for the ill-posed inversion of multi-wavelength lidar data in the retrieval of aerosol size distributions," *Appl. Optics*, vol. 40, pp. 1329–1342, 2001.

[23] G. L. Stephens, R. J. Engelen, M. Vaughan, and T. L. Anderson, "Toward retrieving properties of the tenuous atmosphere using space-based lidar," *J. Geophys. Res.*, vol. 106, pp. 28 143–28 157, 2001.

[24] T. Takamura, Y. Sasano, and T. Hayasaka, "Tropospheric aerosol optical-properties derived from lidar, sun photometer, and optical-particle counter measurements," *Appl. Opt.*, vol. 33, pp. 7132–7141, 1994.

[25] T. Hayasaka, Y. Meguro, Y. Sasano, and T. Takamura, "Optical properties and size distribution of aerosols derived from simultaneous measurements with lidar, a sunphotometer, and an aureolemeter," *Appl. Opt.*, vol. 38, pp. 1630–1635, 1999.

[26] K. J. Voss *et al.*, "Lidar measurements during Aerosols 99," *J. Geophys. Res.*, vol. 106, pp. 20 821–20 832, 2001.

[27] D. Tanré *et al.*, "Measurements and modelization of the Saharan dust radiative impact: Overview of the SaHAran Dust Experiment (SHADE)," J. Geophys. Res., 2003, to be published.

[28] D. Tanré *et al.*, "Climatology of dust aerosol size distribution and optical properties derived from remotely sensed data in the solar spectrum," *J. Geophys. Res.*, vol. 106, pp. 18 205–18 217, 2001.

[29] Y. J. Kaufman *et al.*, "Size distribution and scattering phase function of aerosol particles retrieved from sky brightness measurements," *J. Geophys. Res.*, vol. 99, pp. 10 341–10356, 1994.

[30] D. Tanré *et al.*, "Retrieval of aerosol optical thickness and size distribution over ocean from the MODIS airborne simulator during Tarfox," *J. Geophys. Res.*, vol. 104, pp. 2261–2278, 1999.

[31] J. V. Dave and J. Gazdag, "A modified Fourier transform method for multiple scattering calculations in a plane parallel Mie atmosphere," *Appl. Opt.*, vol. 9, pp. 1457–1466, 1970.

[32] Z. Ahmad and R. S. Fraser, "An iterative radiative transfer code for ocean-atmosphere system," *J. Atmos. Sci.*, vol. 39, pp. 656–665, 1982.

[33] I. Chiapello *et al.*, "Origins of African dust transported over the northeastern tropical Atlantic," *J. Geophys. Res.*, vol. 102, pp. 13 701–13 709, 1997.

[34] X. Li, H. Maring, D. Savoie, K. Voss, and J. M. Prospero, "Dominance of mineral dust in aerosol scattering in the North Atlantic trade winds," *Nature*, vol. 380, pp. 416–419, 1996.

[35] J. M. Prospero and T. N. Carlson, "Vertical and areal distribution of Saharan dust over the western equatorial north Atlantic Ocean," *J. Geophys. Res.*, vol. 77, pp. 5255–5265, 1972.

[36] V. M. Karyampudi *et al.*, "Validation of the Saharan dust plume conceptual model using lidar, Meteosat, and ECMWF data," *Bull. Amer. Meteorol. Soc.*, vol. 80, pp. 1045–1075, 1999.

[37] I. Chiapello *et al.*, "An additional low layer transport of Sahelian and Saharan dust over the north-eastern tropical Atlantic," *Geophys. Res. Lett.*, vol. 22, pp. 3191–3194, 1995.

[38] P. Yang, K. N. Liou, M. I. Mishchenko, and B. C. Gao, "Efficient finite-difference time-domain scheme for light scattering by dielectric particles: Application to aerosols," *Appl. Opt.*, vol. 39, pp. 3727–3737, 2000.
[39] D. M. Winker and B. A. Wielicki, "The PICASSO-CENA Mission in sensors, systems, and next generation satellites," *Proc. SPIE*, vol. 3870, p. 2636, 1999.
[40] M. I. Mishchenko, L. D. Travis, R. A. Kahn, and R. A. West, "Modeling phase functions for dustlike tropospheric aerosols using a shape mixture of randomly oriented polydisperse spheroids," *J. Geophys. Res.*, vol. 102, pp. 16 831–16 847, 1997.
[41] E. Hamonou *et al.*, "Characterization of the vertical structure of Saharan dust export to the Mediterranean basin," *J. Geophys. Res.*, vol. 104, pp. 22 257–22 270, 1999.
[42] I. Mattis, A. Ansmann, D. Muller, U. Wandinger, and D. Althausen, "Dual-wavelength Raman lidar observations of the extinction-to-backscatter ratio of Saharan dust," *Geophys. Res. Lett.*, vol. 29, pp. 1306–1309, 2002.
[43] Y. J. Kaufman, D. Tanré, O. Dubovik, A. Karnieli, and L. A. Remer, "Absorption of sunlight by dust as inferred from satellite and ground-based remote sensing," *Geophys. Res. Lett.*, vol. 28, pp. 1479–1483, 2001.
[44] D. M. Winker, R. H. Couch, and M. P. McCormick, "An overview of LITE: NASA's lidar in-space technology experiment," *Proc. IEEE*, vol. 84, no. 2, pp. 164–180, 1996.
[45] T. L. Anderson, R. J. Charlson, D. M. Winker, J. A. Ogren, and K. Holmen, "Mesoscale variations of tropospheric aerosols," *J. Atmos. Sci.*, vol. 60, pp. 119–136, 2003.
[46] J.-L. Deuzé *et al.*, "Estimate of the aerosol properties over the ocean with POLDER," *J. Geophys. Res.*, vol. 105, pp. 15 329–15 346, 2000.
[47] J.-L. Deuzé *et al.*, "Remote sensing of aerosol over land surfaces from POLDER-ADEOS-I polarized measurements," *J. Geophys. Res.*, vol. 106, pp. 4913–4926, 2001.
[48] J. D. Klett, "Stable analytical inversion solution for processing lidar return signal," *Appl. Opt.*, vol. 20, pp. 211–220, 1981.
[49] C. Flamant, V. Trouillet, P. Chazette, and J. Pelon, "Wind speed dependence of atmospheric boundary layer optical properties and ocean surface reflectance as observed by airborne backscatter lidar," *J. Geophys. Res.*, vol. 103, pp. 25,137–25 158, 1998.

Yoram J. Kaufman received the B.S. and M.S. degrees in physics from the Technion—Israeli Institute of Technology, Haifa, Israel, and the Ph.D. degree from the Tel-Aviv University, Tel Aviv, Israel.

He came to NASA Goddard Space Flight Center (GSFC), Greenbetl, MD, in 1979 on an NRC Fellowship Award. He is currently a Senior Fellow and Atmospheric Scientist at GSFC. He has served as the Project Scientist of the Earth Observing System first satellite EOS-Terra, from 1996 through its launch in December 1999, and was a Member of the MODIS Science Team (1988–2003). His present work includes theoretical and experimental research in atmospheric radiative transfer and remote sensing of aerosol, their interaction with clouds and radiation, and impact on climate. He conducted the Smoke/Sulfate, Clouds And Radiation (SCAR) field experiments in Brazil and the United States (1993–1995), to characterize smoke aerosol properties, their emissions from fires, and their effect on clouds and radiation. He has over 150 refereed publications.

Dr. Kaufman is the seventh recipient of the NASA/GSFC Nordberg Award for Earth Sciences and was awarded the NASA Medal for Exceptional Scientific Achievement.

Didier Tanré received the M.S. degree in physics in 1975 and the "Thèse de 3ème Cycle"and the "Doctorat d'Etat" in atmospheric physics in 1977 and 1982, respectively, all from the Université des Sciences et Techniques de Lille, Lille, France.

He is currently an Atmospheric Scientist in the Centre National de la Recherche Scientifique (CNRS), Toulouse, France, collocated with the Laboratoire d'Optique Atmosphérique at the Université des Sciences et Technologies de Lille, France, where he has been a Research Scientist since 1982. He is a Member of the MODIS Science Team, where he has primary responsibility for remote sensing of tropospheric aerosol over the ocean. He is the Principal Investigator of the PARASOL mission. He is currently the Director of the Laboratoire d'Optique Atmosphérique at the Université des Sciences et Technologies de Lille.

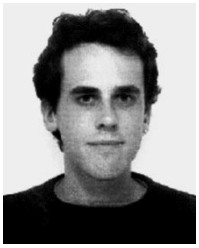

Jean-François Léon was born in Saint-Brieuc, France, in 1973. He received the Ph.D. degree in atmospheric science and air pollution chemistry from Paris VII University, Paris, France in 2000.

He came to Laboratoire d'Optique Atmosphérique, Lille, France, in 2001 on a Centre National d'Etudes Spatiale (CNES) Fellowship. He is currently an Associate Professor at the Université Lille I, Lille France. His experience is principally in the area of aerosol remote sensing. His research interests concern the cycle of aerosols in the atmosphere and their interactions with the radiative budget, and the regional and global climate.

Jacques Pelon graduated from Ecole Supérieure d'Electricité, France, in 1977, and received the Docteur es Sciences degree in physics from University Pierre et Marie Curie, Paris, France, in 1985.

He joined the Centre National de la Recherche Scientifique (CNRS), Toulouse, France, in 1984. He is Directeur de Recherche at Service d'Aéronomie and associated with the Laboratoire de Météorologie Dynamique (both part of Institut Pierre Simon Laplace). His research field is related to dynamics and radiation budget in the lower atmosphere. He is currently working on the application of active optical remote sensing using lidar systems for the characterization of aerosol properties and aerosol–cloud interactions. He is Principal Investigator (PI) for the French airborne lidar program LEANDRE and co-PI for the space mission CALIPSO jointly developed by NASA and CNES. He has over 70 publications in international journals with peer review.